CrossMark

ORIGINAL PAPER

A simplified hardening cohesive zone model for bondline thickness dependence on adhesive joints

Yongtao Sun · Nicola Pugno · Baoming Gong · Qian Ding

Abstract In this paper, a tri-material adhesive system with nonlinear cohesive springs embedded between two elasto-plastic adhesive layers is proposed to predict the adhesive thickness effects on the fracture energy of bonded joints. The localized plastic and damage behaviours along the interface are described by the hardening cohesive zone models. The thickness dependent interfacial energy release rate is divided into the essential separation energy rate and the energy dissipation rate of the plasticization. The adhesive thickness dependent hardening cohesive zone model is implemented into the proposed numerical method to predict the failure of the adhesive joints. The validation of the model is performed by comparison with the experimental data.

Y. Sun · Q. Ding
Department of Mechanical Engineering, Tianjin
University, Tianjin 300072, China

N. Pugno
Laboratory of Bio-Inspired & Graphene Nanomechanics,
Department of Civil, Environmental and Mechanical
Engineering, Università di Trento, 38123 Trento, Italy

N. Pugno
Center for Materials and Microsystems, Fondazione Bruno
Kessler, 38123 Povo (Trento), Italy

N. Pugno
School of Engineering and Materials Science, Queen Mary
University of London, London E1 4NS, UK

B. Gong (✉)
Department of Materials Science and Engineering, Tianjin
University, Tianjin 300072, China
e-mail: gongbm@tju.edu.cn

1 Introduction

Adhesive joints are being widely used in industries, e.g., in the automotive and aerospace industries. Some specimens have been used to examine the fracture properties of adhesive joints, including double cantilever beam (DCB) (Mall and Ramamurthy 1989; Abou-Hamda et al. 1998; Chai 1988, 1986; Bascom et al. 1975; Kinloch and Shaw 1981; Hunston et al. 1989), compact tension (CT) (Daghiyani et al. 1995), peel tests (Kawashita et al. 2008; Pardoen et al. 2005). Through these tests, a significant fracture strength and toughness improvement by increasing adhesive thickness has been widely observed (Abou-Hamda et al. 1998; Chai 1986; Bascom et al. 1975; Kinloch and Shaw 1981; Daghiyani et al. 1995; Kawashita et al. 2008; Pardoen et al. 2005). Therefore, from the point view of design, an interpretation of bondline thickness effects on the fracture behaviour of adhesive joints is instructive to optimize the global properties. Linear Elastic Fracture Mechanics (LEFM) and the interfacial fracture mechanics are introduced to predict the failure of the adhesive joint, and the Cohesive Zone Model (CZM) proposed by Barenblatt (1959), Barenblatt (1962) and Dugdale (1960) was proven to be versatile to study crack propagation in interface problems. To solve different fracture problems, several shapes of the CZM

are proposed, namely the linear softening shape (Barenblatt 1962; Dugdale 1960), the trapezoidal shape (Bilby et al. 1963), as well as the bell-shapes or exponential forms (Willis 1967; Wnuk 1974; Hillerborg et al. 1976). In spite of this remarkable development of the nonlinear fracture mechanics models, the shape of the CZM and its input parameters are often obtained by fitting the experimental data or by inverse analysis (Burke et al. 2007; Valoroso and Fedele 2010; Gain et al. 2011; Shen and Paulino 2011; Chen et al. 2014). Moreover, the cohesive law is considered as the equivalent interfacial traction-separation to describe the interaction across the adherents, and many experiments have indicated that the cohesive law may be thickness dependent due to the plastic zone size and deformation magnitude in the adhesive material (Azari et al. 2011). As a result, the cohesive laws for different geometric joints have to be calibrated through different experiment data, and the transferability of the CZM parameters is seriously limited. The aim of this paper is thus to apply the simplified hardening cohesive zone model to estimate the adhesive thickness dependent effect on the fracture of the bonded joints, where the cohesive parameters are obtained explicitly from the tensile properties of the adhesive.

2 The hardening cohesive law

2.1 Basic concepts of the cohesive zone model

The basic assumption of the cohesive zone model is the formation, as an extension of the real crack, of a fictitious crack, referred to as the process zone, where the material, albeit damaged, is still able to transfer stresses. In the process zone, the stresses transferred by the material are functions of the displacement discontinuity, according to a proper cohesive law, whilst in the uncracked zone the behaviour of the material is linear-elastic or elasto-plastic. Some cohesive crack models may share the common character that the cohesive traction at the fictitious tip is zero. However, from a physical point of view, the cohesive law describes the progressive fracture process induced by finite deformation or applied stress. It is thus reasonable that the initial value of the traction versus separation law should be different from zero (Carpinteri et al. 2012). Mathematically, the cohesive law with an initial zero traction does not guarantee the absence of stress singularity at the fictitious

crack tip (Jin and Sun 2005). Moreover, the cohesive law of the adhesive joints is usually thickness dependent on the process zone size and the localized plastic deformation magnitude (Azari et al. 2011). In particular, the volumetric plastic energy dissipation rate is thickness dependent. Therefore, it is reasonable to postulate that the equivalent interfacial energy release rate comprises the energy dissipation referred to the plasticization of the material surrounding the process zone and the separation energy rate required to create new fracture surfaces.

2.2 Derivation of the hardening cohesive law

It is assumed in the present work that the localized plastic and damage behaviour of the adhesive joints are described by hardening cohesive zone model where localized plastic dissipation and crack formation and propagation take place Carpinteri et al. (2012). Accordingly, the mechanical behaviour of the adhesive joints under uniaxial tension can be divided into the following stages:

(a) Homogeneous elastic deformation in adhesive bulk: the materials behave linear elastically without any damage or localized zone (see Fig. 1a). The constitutive law is that shown in Fig. 1a, and the elongation δ is

$$\delta = \varepsilon L = \frac{\sigma L}{E_{adhesive}}, \quad \text{for } \sigma \leq \sigma_y. \tag{1}$$

(b) Localized plastic deformation in the adhesive layer: after the elastic limit of the adhesive material, the deformation starts to localize and give rise to the localized plasticity within a limited portion of the adhesive (Fig. 1b). In the present work a simplified linear hardening plasticity is assumed. Thus, the linear hardening cohesive traction-elongation relationship is given by

$$\delta = \frac{\sigma - \sigma_y}{k_1}, \quad \text{for } \sigma_f > \sigma > \sigma_y. \tag{2}$$

(c) Crack formation of the adhesive: as the localized plastic deformation proceeds, microvoid enlargement and coalescence in the polymer leads to the softening behaviour, and the branch is provided as

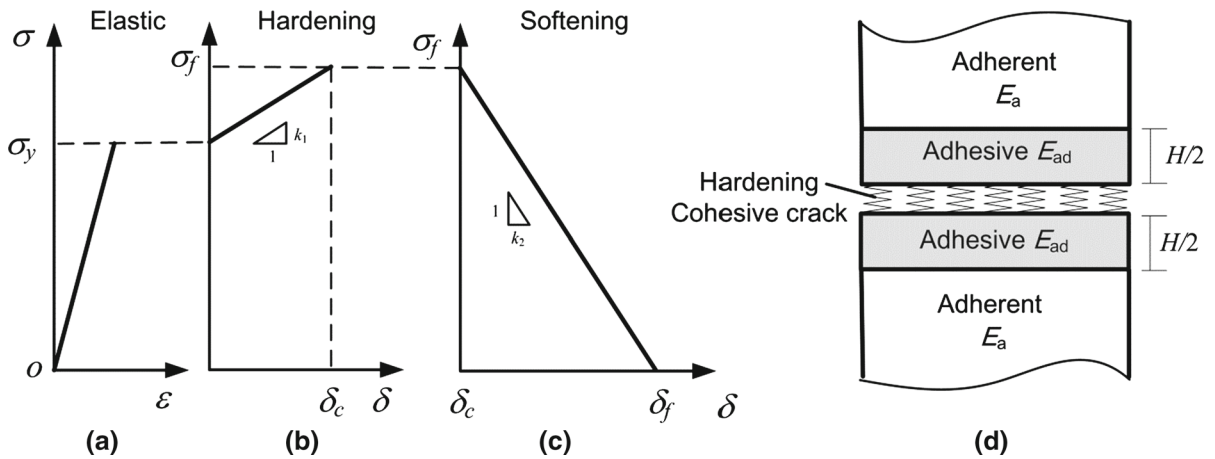$$\sigma = (\delta_f - \delta) k_2, \quad \text{for } \delta_c < \delta \leq \delta_f. \tag{3}$$

Fig. 1 The simplified hardening cohesive law and the tri-material adhesive system for the adhesive joints

where k_1 and k_2 are two cohesive shape parameters obtained by the best-fitting experimental data, while the shape determined by k_1 and k_2 has only a slight influence on mechanical behavior as claimed by Tvergaard and Hutchinson (1992).

3 The equivalent thickness dependence behaviour of the adhesive joints

In this paper, it is assumed that a tri-material adhesive system equivalently composes of the virtual spring

deformation of the adhesive and the nonlinear spring. For adhesive of the DBC specimen, it is assumed that the adhesive and the cohesive zone act as springs in series (Kanninen 1973; Penado 2006; Williams and Hadavinia 2002). Paggi and Wriggers (2011) recently captured the finite thickness interface properties in the nonlocal cohesive zone model using the similar strategy. In this case, the total displacement of the system is the sum of the individual contributions. The relationship between the traction σ and the cohesive opening δ of the adhesive can be distinguished into three different stages:

$$\begin{cases} \text{Homogeneous elastic deformation}: \sigma = E_{adhesive}\varepsilon & \text{for } 0 < \varepsilon \le \varepsilon_y \\ \text{Hardening phase}: \sigma = \dfrac{\left(\Delta + \frac{\sigma_y}{k_1}\right)}{\left(\frac{H}{2E_{adhesive}} + \frac{1}{k_1}\right)} + \sigma_y \dfrac{\frac{H}{2E_{adhesive}}}{\left(\frac{H}{2E_{adhesive}} + \frac{1}{k_1}\right)} & \text{for } 0 < \delta \le \delta_c \ . \\ \text{Softening phase}: \Delta = \left(\frac{\sigma}{2E_{adhesive}}H\right) + \left(\delta_f - \frac{\sigma}{k_2}\right) & \text{for } \delta > \delta_c \end{cases} \tag{4}$$

embedded between two adhesive layers with modulus E_{adhesvie} and the half thickness $H/2$ (see Fig. 1d). The adhesive layers refer to the diffuse plasticization of the material surrounding the process zone, and the localized deformation and separation to create new fracture surfaces are represented by the nonlinear springs. The spring is constituted according to the hardening cohesive law, and its volume is assumed to be zero for the weak interface, and a linear hardening plasticity for the adhesive layer. The bi-material interface between adhesive and spring is perfectly bonded. The separation of the adhesive system under loading is the sum of the

where σ_y and σ_f is the yielding strength and tensile strength of the bulk adhesive, respectively. The equivalent fracture energy in the adhesive can be determined as

$$G_{Ic} = \int_0^{\delta_c} \sigma\,(\delta)\,d\delta + \int_{\delta_c}^{\delta_f} \sigma\,(\delta)\,d\delta, \ \delta_y = \frac{\sigma_y H}{E_{adhesive}}. \tag{5}$$

Substituting Eq. (4) into Eq. (5), we can obtain

Fig. 2 The two-node, zero-thickness interface elements and the numerical implementation
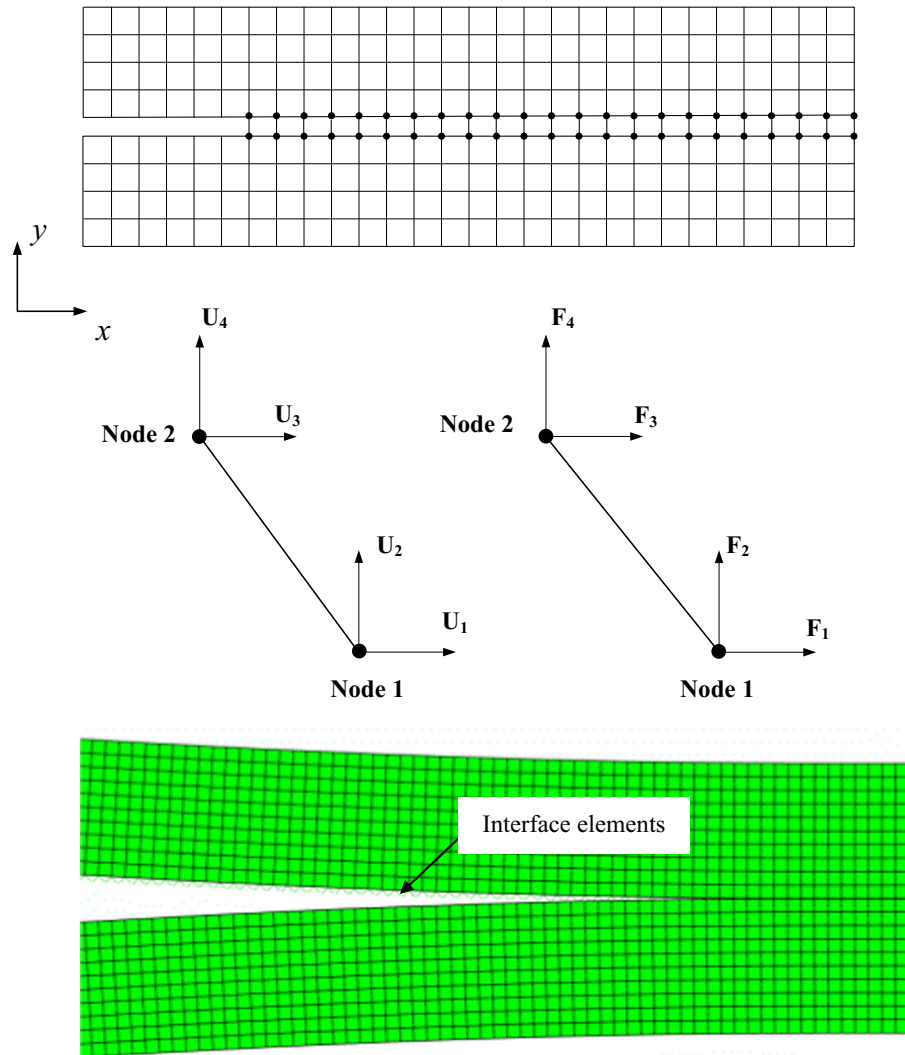
G_{Ic}
$$= \left\{ \left(\frac{\sigma_f + \sigma_y}{2} \right) \left[\sigma_f \left(\frac{H}{2E_{adhesive}} + \frac{1}{k_1} \right) - \frac{H}{2E_{adhesive}} \sigma_y \right] \right.$$
$$\left. - \left(\frac{\sigma_f + \sigma_y}{2} \right) \frac{\sigma_y}{k_1} \right\} + \frac{1}{2} \sigma_f^2 \left(\frac{H}{2E_{adhesive}} - \frac{1}{k_2} \right). \quad (6)$$

Considering the energy dissipation in both volume and the hardening cohesive zone, Eq. (6) can be alternatively rewritten as

$$G_{Ic} = G_H + G_{cohesive}. \quad (7)$$

where G_H is the volumetric plastic energy dissipation rate and is thickness dependent, $G_{cohesive}$ is the generalized Griffith energy. Comparing Eq. (7) with Eq. (6),

the following expressions can be directly obtained

$$G_H = \left(\frac{H}{2E_{adhesive}} \right) \left(2\sigma_f^2 - \sigma_y^2 \right). \quad (8a)$$

$$G_{cohesive} = \frac{\sigma_f^2 - \sigma_y^2}{2k_1} - \frac{\sigma_f^2}{2k_2} = constant. \quad (8b)$$

It is obvious in Eq. (7) that the nominal fracture energy is approximately proportional to the adhesive thickness, and $G_{cohesive}$ can be determined from the fracture toughness corresponding to a reference bondline thickness. Taking constraint effects into consideration, Yan et al. (2001) obtained the similar result that $G = C_m \sigma_f H$ (C_m is a constraint constant depending on the ultimate stress). Once $G_{cohesive}$ is obtained by the

experimental fitting, k_1 and k_2 are dummy parameters which are not necessarily known.

4 Numerical implementation and experimental validation

The commercial code ABAQUS/Standard is used for the debonding simulations. The weak interface is represented by 2-node, zero-thickness interface elements in a user-defined subroutine (UEL). On the basis of the equivalent constitutive laws previously introduced for joints, the fracturing along the interface between two adherents can be described by means of the discrete nodal release approach proposed by Carpinteri et al. for reinforced concrete beams (Yan et al. 2001) and ductile fracture (Carpinteri et al. 2012). In this scheme, the hardening cohesive zone model is applied in conjunction with nonlinear spring type elements. The cohesive law is implemented as the spring force vs. displacement separation according to the constitutive laws in Eq. (4).

Since the element has two nodes and each node has two degree of freedom for the two-dimensional analysis, the current nodal displacement vector within ABAQUS user subroutine UEL is $\{U_1, U_2, U_3, U_4\}$. The displacement components for node 1 are U_1 and U_2 in the x and y directions, respectively. Similarly, U_3 and U_4 are the displacement components for node 2 as shown in Fig 2. Considering the linear hardening and softening branches in the traction-separation law, the nodal forces $\{F_1, F_2, F_3, F_4\}$ can be obtained as follows

$$\left\{ \begin{array}{c} F_1 \\ F_2 \\ F_3 \\ F_4 \end{array} \right\} = KU = \left[\begin{array}{cccc} k_{ix} & 0 & -k_{ix} & 0 \\ 0 & k_{iy} & 0 & -k_{iy} \\ -k_{ix} & 0 & k_{ix} & 0 \\ 0 & -k_{iy} & 0 & k_{iy} \end{array} \right] \left\{ \begin{array}{c} U_1 \\ U_2 \\ U_3 \\ U_4 \end{array} \right\};$$

(9)

where k_{ix} and k_{iy} are values of the cohesive stiffness corresponding to different branches in the traction-separation law Carpinteri et al. (2012); K is the stiffness matrix assigned to the AMATRX in the UEL subroutine; U is the nodal displacement vector. It is worth noting that the same numerical algorithm can be profitably used with the nonlinear cohesive law through the multi-segment method where the nonlinear traction-separation law is approximated by multiple linear relations. The beams are discretized with standard full inte-
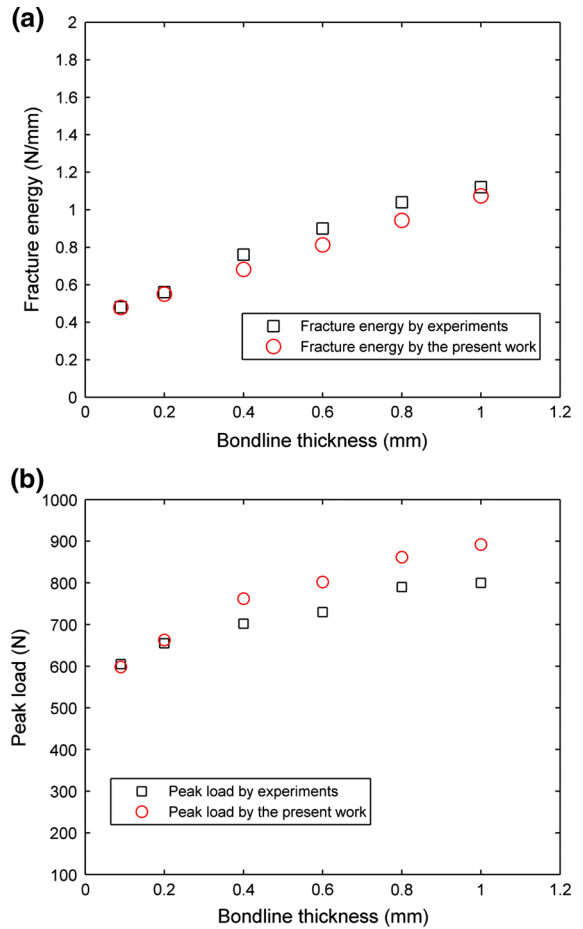

Fig. 3 Effect of the bondline thickness on **a** cohesive energy and **b** peak load by experiments and the present work for $H=0.09$, 0.2, 0.4, 0.6, 0.8, and 1.0 mm

gration four-node 2D plane strain elements (CPE4), and uniform-sized cohesive elements are inserted along the horizontal direction, which corresponds to the potential crack path. In the numerical model, we insert 330 user-define cohesive elements along the interface of the DCB, which is enough to simulate the failure process efficiently. The total length these elements is 210 mm, and the size of the uniform cohesive element is 0.635 mm. The finite element model has 8318 elements and 318 cohesive elements. The meshes are shown in Fig.3. Additionally, a modified Riks method is utilized to capture post-peak load behavior. Fixed displacement boundary conditions are employed at the ends of the beams.

The proposed simplified hardening cohesive law is examined through application to analyze the experi-

Fig. 4 The normalized hardening cohesive law for $h = 0.09, 0.2, 0.4, 0.6, 0.8,$ and 1.0 mm (**a**); the load versus displacement curve by experiment and the present work (**b**); contours of S22 stress of DCB with different adhesive thickness under Mode I at peak loading (**c**)
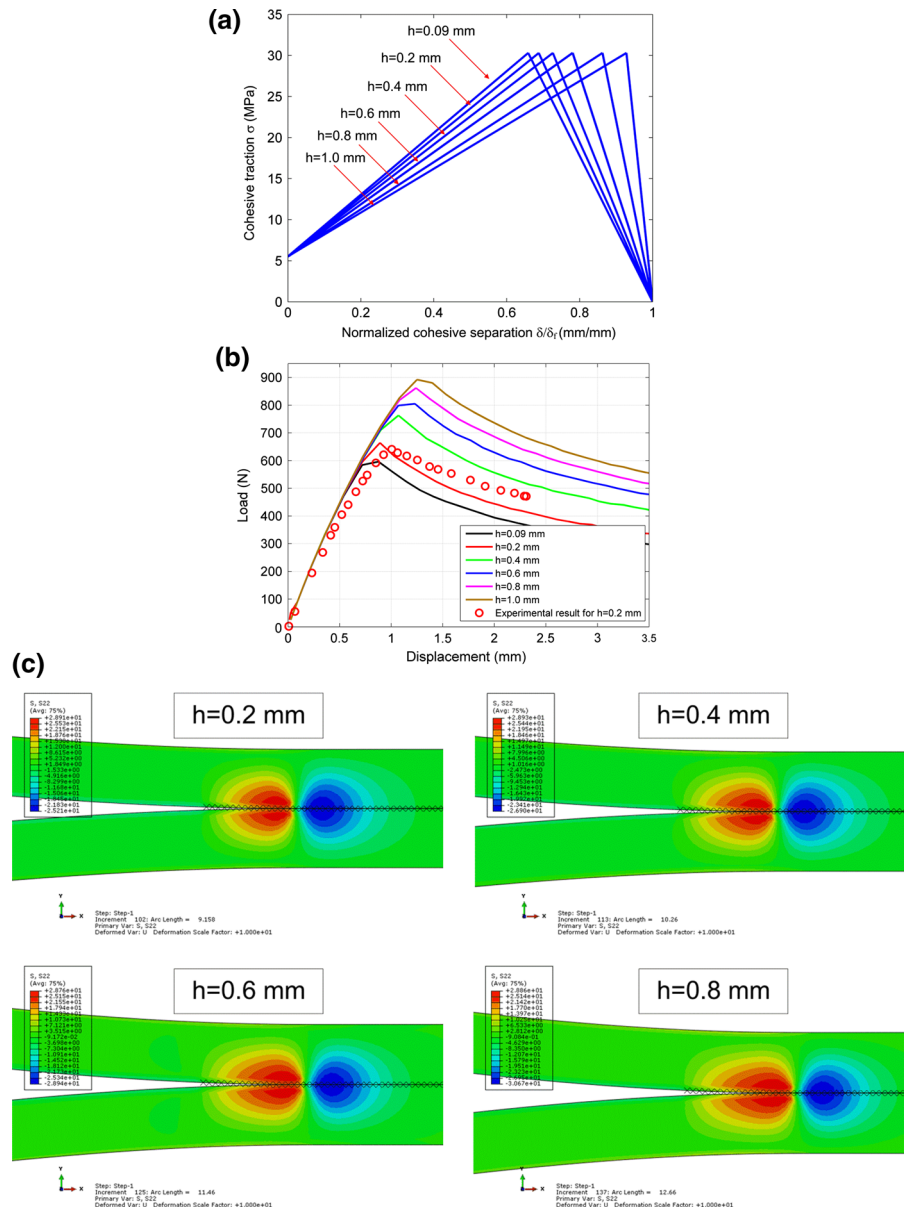
mental results from Ji et al. (2010). They employed DCB to investigate the effect of adhesive thickness on interfacial energy release rate, interfacial strength, and shapes of the interfacial traction-separation laws. The actual average adhesive thicknesses of the six groups of specimens are 0.09, 0.2, 0.4, 0.6, 0.8, and 1.0 mm, respectively. Ultimate stress σ_f of the adhesive material (LOCTITE Hysol 9460) is 30.3 MPa which is provided by the manufacturer; the yield stress σ_y is corresponding to the stress at 0.2 % plastic strain; the elongation rate 3.5 % refers to deformation at the final

rupture. Low carbon steel adherents are used to fabricate the 6.35 mm thick, 25.4 mm wide and 254 mm long adherends of DCB specimens with initial crack length 52.2 mm.

According to Eqs. (6)–(8b), the fracture energies for six thickness adhesive joints are determined analytically in Fig. 3a. Furthermore, the numerical load-deflection curves for the joint with different bondline thicknesses are obtained, where the maximum load can be determined. The comparison with all the experiments in terms of cohesive energy and peak load is

shown in Fig. 3a, b, where a very good approximation is plotted for all the considered bondline thicknesses. As an example, the load-deflection curve for the joint with a 0.2 mm thick adhesive layer predicted by the hardening cohesive law is plotted against the experiment in Fig. 4b for comparison. In addition, the normalized cohesive law, the others load-deflection responses and the distribution of S22 stress at peak loading for $h = 0.2$, 0.4, 0.6, 0.8 mm are also plotted in Fig. 4a–c, respectively.

5 Discussion

In this paper, a simplified hardening cohesive law is proposed to predict the adhesive thickness effect on the fracture behaviours of bonded joints. Accordingly, the thickness dependent interfacial energy release rate is comprised of the separation energy rate and the plastic energy dissipation rate. More specifically, the hardening cohesive energy can be divided into G_H, the volumetric plastic energy dissipation rate and thickness dependent, and $G_{cohesive}$, the generalized Griffith energy. As a result, the present analyses indicate that the nominal fracture energy is approximately proportional to the adhesive thickness, which is in consistent with the suggestion by Yan et al. (2001). Taking constraint effects into consideration, they obtained the similar result (Yan et al. 2001).

Regarding to the relationship between the horizontal displacement and the applied shear traction, the sliding behaviour can be identified through the same tri-material system. For the mixed mode, we can use the dimensionless separation parameter to couple the opening and sliding modes (Tvergaard and Hutchinson 1992; Paggi and Wriggers 2011). On the other hand, we assume a constant cohesive strength for approximation so that in the hardening cohesive law for a thin layer, the failure is prone to strength-controlled since the hardening branch becomes steeper; for a thick layer, the hardening branch is descended more gently, which is deformation-controlled failure (see Fig. 4a). In general, the critical cohesive parameters are considered to depend on the stress-state (Yan et al. 2001; Siegmund and Brocks 2000). Experimental results indicate different tendencies that fracture energy increases (Chai 2004) or decreases (Bascom et al. 1975; Chai 1986) or increases followed by decreasing (Kinloch and Shaw 1981) as the bond thickness is increased. For the case,

fracture is mainly controlled by a critical opening stress dependent on the stress tri-axiality or constraint parameters. As the thickness increases, critical crack tip opening displacement is a more suitable fracture criterion, and the fracture toughenss of the joint asymptotically approaches the bulk value. In fact, the apparent size effect on fracture energy and strength of adhesive joint is actually determined by interactions between process zone and boundary conditions, or the distance between the crack-tip to the boundary of the structure. From the micromechanical point of view, two competing fracture mechanisms can be assumed for a constrained adhesive layer in rigid adherends. In a very thin adhesive layer, cavitation ahead of the crack tip may precede plastic flow, and the fracture is dominated by high triaxial stresses; otherwise, crack tip blunting may result in void-crack coalescence in a thick adhesive layer. Thus, the models for thin and thick adhesive should be considered separately to determine the comprehensive adhesive-thickness dependent fracture behaviours as suggested in Duan et al. (2004).

References

Abou-Hamda MM, Megahed MM, Hammouda MMI (1998) Fatigue crack growth in double cantilever beam specimen with an adhesive layer. Eng Fract Mech 60:605–614

Azari S, Papini M, Spelt JK (2011) Effect of adhesive thickness on fatigue and fracture of toughened epoxy joints–Part II: analysis and finite element modeling. Eng Fract Mech 78:138–152

Barenblatt GI (1959) The formation of equilibrium cracks during brittle fracture: general ideas and hypotheses. J Appl Math Mech 23:622–636

Barenblatt GI (1962) The mathematical theory of equilibrium cracks in brittle fracture. Adv Appl Mech 7:55–129

Bascom WD, Cottington RL, Jones RL, Peyser P (1975) The fracture of epoxy and elastomer-modified epoxy polymers in bulk and as adhesives. J Appl Polym Sci 19:2545–2562

Bilby BA, Cottrell AH, Swinden KH (1963) The spread of plastic yield from a notch. Proc R Soc Lond A 272:304–314

Burke BCP, Kim SO, Kim KS (2007) Partial polar decomposition inverse method applied to determination of internal stresses in an elastic complex structure. Int J Solids Struct 44:2010–2020

Carpinteri A, Corrado M, Paggi M, Mancini G (2009) New model for the analysis of size-scale effects on the ductility of reinforced concrete elements in bending. J Eng Mech (ASCE) 135:221–229

Carpinteri A, Gong B, Corrado M (2012) Hardening cohesive/overlapping zone model for metallic materials: the size-scale independent constitutive law. Eng Fract Mech 82:29–45

Chai H (1986) Bond thickness effect in adhesive joints and its significance for mode I interlaminar fracture of composites. Composite materials testing and design, ASTM STP 893:209–231

Chai H (1988) Fracture work of thin bondline adhesive joints. J Mater Sci Lett 7:399–401

Chai H (2004) The effects of bond thickness, rate and temperature on the deformation and fracture of structural adhesives under shear loading. Int J Fract 130:497–515

Chen X, Deng X, Sutton MA, Zavattieri P (2014) An inverse analysis of cohesive zone model parameter values for ductile crack growth simulations. Int J Mech Sci 79:206–215

Daghiyani HR, Ye L, Mai Y-W (1995) Mode-I fracture behaviour of adhesive joints part I. relationship between fracture energy and bond thickness. J Adhes 53:149–162

Duan Kai, Xiaozhi Hu, Mai Yiu-Wing (2004) Substrate constraint and adhesive thickness effects on fracture toughness of adhesive joints. J Adhes Sci Technol 18:39–53

Dugdale DS (1960) Yielding of steel sheets containing slits. J Mech Phys Solids 8:100–104

Gain AL, Carroll J, Paulino GH, Lambros J (2011) A hybrid experimental/numerical technique to extract cohesive fracture properties for mode-I fracture of quasi-brittle materials. Int J Fract 169:113–131

Hillerborg A, Modeer M, Petersson PE (1976) Analysis of crack formation and crack growth in concrete by means of fracture mechanics and finite elements. Cem Concr Res 6:773–782

Hunston DL, Kinloch AJ, Wang SS (1989) Micromechanics of fracture in structural adhesive bonds. J Adhes 28:103–114

Ji G, Ouyang Z, Li G, Ibekwe S, Pang S (2010) Effects of adhesive thickness on global and local Mode-I interfacial fracture of bonded joints. Int J Solids Struct 47:2445–2448

Jin Z-H, Sun CT (2005) Cohesive fracture model based on necking. Int J Fract 134:91–108

Kanninen MF (1973) An augmented double cantilever beam model for studying crack propagated and arrest. Int J Fract 9:83–92

Kawashita LF, Kinloch AJ, Moore DR, Williams JG (2008) The influence of bond line thickness and peel arm thickness on adhesive fracture toughness of rubber toughened epoxy-aluminium alloy laminates. Int J Adhes Adhes 28:199–210

Kinloch AJ, Shaw SJ (1981) The fracture resistance of a toughened epoxy adhesive. J Adhes 12:59–77

Mall S, Ramamurthy G (1989) Effect of bond thickness on fracture and fatigue strength of adhesively bonded composite joints. Int J Adhes 9:33–37

Paggi M, Wriggers P (2011) A nonlocal cohesive zone model for finite thickness interfaces-Part I: mathematical formulation and validation with molecular dynamics. Comput Mater Sci 50(5):1625–1633

Pardoen T, Ferracin T, Landis CM, Delannay F (2005) Constraint effects in adhesive joint fracture. J Mech Phys Solids 53:1951–1983

Penado FE (2006) A closed form solution for the energy release rate of the double cantilever beam specimen with an adhesive layer. J Compos Mater 40(8):701–715

Shen B, Paulino GH (2011) Direct extraction of cohesive fracture properties from digital image correlation: a hybrid inverse technique. Exp Mech 51:143–163

Siegmund T, Brocks W (2000) A numerical study on the correlation between the work of separation and the dissipation rate in ductile fracture. Eng Fract Mech 67:139–154

Tvergaard V, Hutchinson JW (1992) The relation between crack growth resistance and fracture process parameters in elastic-plastic solids. J Mech Phys Solids 40:1377–1397

Valoroso N, Fedele R (2010) Characterization of a cohesive-zone model describing damage and de-cohesion at bonded interfaces. Sensitivity analysis and mode-I parameter identification. Int J Solids Struct 47:1666–1677

Williams J, Hadavinia H (2002) Analytical solutions for cohesive zone models. J Mech Phys Solids 50:809–825

Willis JR (1967) A comparison of the fracture criteria of Griffith and Barenblatt. J Mech Phys Solids 15:151–162

Wnuk MP (1974) Quasistatic extension of a tensile crack contained in viscoelastic-plastic solid. J Appl Mech 41:234–242

Yan C, Mai Y-W, Lin Y (2001) Effect of bond thickness on fracture behaviour in adhesive joints. J Adhes 75(1):27–44